DOI: http://dx.doi.org/10.15446/ing.investig.v35n2.49838

HDO of guaiacol over NiMo catalyst supported on activated carbon derived from castor de-oiled cake

HDO del guaiacol mediante el uso de catalizadores NiMo soportados sobre carbón activado obtenido a partir de la torta de higuerilla

V. Ospina[1], R. Buitrago-Sierra[2], and D. López[3]

ABSTRACT

Physical and chemical activation methods were used to prepare two different activated carbons (ACs) from castor de-oiled cake. H_2O/CO_2 mixture was used as the physical activating agent, and for chemical activation potassium carbonate (K_2CO_3) was used. For both materials, textural and chemical properties were characterized by N_2 adsorption–desorption isotherms, thermogravimetric analysis (TGA), Fourier Transform Infrared Spectroscopy (FTIR), thermal programmed reduction (TPR), X-ray fluorescence (XRF), and scanning electron microscopy (SEM). The ACs were used as supports for NiMo sulfide catalysts, which were prepared by wetness impregnation and in-situ sulfided for the hydrodeoxygenation (HDO) of guaiacol (GUA) as a model compound of bio-oil. The HDO reaction was carried out in a typical batch reactor at 5 MPa of H_2 and 350 °C. Under the same test conditions, commercial catalysts were also tested in the reaction. Although the commercial catalysts displayed higher GUA conversion, the prepared catalysts showed higher activity and non-oxygenated and saturated products yield.

Keywords: Castor de-oiled cake, activated carbon, hydrodeoxygenation, bio-oils.

RESUMEN

Se prepararon dos carbones activados a partir de la torta de higuerilla; como métodos para su obtención se usaron la activación física y la activación química. Para la activación física se usó una mezcla H_2O/CO_2 como agente activante, y para la activación química, K_2CO_3. Las propiedades químicas y texturales de ambos carbones activados fueron caracterizados por isotermas de adsorción-desorción de N_2, análisis termogravimétrico (TGA), espectroscopia infrarroja (FT-IR), reducción a temperatura programada (TPR), fluorescencia de rayos X (XRF) y microscopía electrónica de barrido (SEM). Los carbones activados se usaron como soporte en catalizadores NiMo sulfurados, los cuales fueron preparados por impregnación húmeda y reducidos in-situ para la reacción de hidrodesoxigenación del guaiacol (GUA), compuesto modelo de los aceites de pirólisis. La reacción de hidrodesoxigenación (HDO) se realizó en un reactor tipo batch a 5 MPa de H_2 y 350 °C. Con el fin de comparar, los catalizadores comerciales también se probaron en reacción. A pesar de que los catalizadores comerciales mostraron una mayor conversión de GUA, los catalizadores sintetizados exhibieron una mayor actividad y un mayor rendimiento en la producción de compuestos saturados y no oxigenados.

Palabras clave: Torta de higuerilla, carbón activado, hidrodesoxigenación, bioaceites.

Received: March 27th 2015
Accepted: May 9th 2015

Introduction

Thermochemical conversion processes, such as pyrolysis, have been used over biomass for energy recovery (Abdullah, Sulaiman, & Gerhauser, 2011; Bridgwater, 2011) and production of some materials as activated carbons (ACs) (González, Román, Encinar, & Martínez, 2009; Kazehaya, Muroyama, & Watkinson, 2000). Although ACs may be produced from coal or petroleum coke, there is a special interest in biomass wastes as feedstock (Ioannidou & Zabaniotou, 2007), since they are inexpensive raw materials and they have minimal negative environmental impact.

Activated carbons have a wide range of applications, particularly as adsorbent and catalyst support (Serp & Figueredo, 2009). Activated carbons used in catalysis exhibit a specific pore volume between 0.9 and 1.3 cm^3/g and surface areas from 800 to 1200 m^2/g (Auer, Freund, Pietsch, & Tacke, 1998). One key advantage of using activated carbon as catalyst support, in addition to its low cost, is the benefit of obtaining a large surface area that maximizes the exposed area of the active phase. Physical and chemical activations are the two principal methods to produce activated carbon from biomass (Marsh & Rodriguez-reinoso, 2006). In physical activation, after the pyrolysis of biomass, pore formation is favored by reaction between char and oxidizing gases like steam, CO_2, or a mixture of them. In chemical activation, the biomass is treated with substances like $ZnCl_2$, H_3PO_4, KOH or K_2CO_3, which create porosity by promoting oxidation or dehydration reactions in the cellu-

[1] Viviana María Ospina: Chemist, Universidad de Antioquia, Medellín, Colombia. E-mail: viviana.ospina@udea.edu.co

[2] Robison Buitrago Sierra: Chemist, PhD Materials Science. Affiliation: Docente Investigador, Instituto Tecnológico Metropolitano, Medellín, Colombia. E-mail: robinsonbuitrago@itm.edu.co

[3] Diana Patricia López: Chemist, PhD Chemistry. Affiliation: Docente Investigador, Universidad de Antioquia, Medellín, Colombia. E-mail: diana.lopez@udea.edu.co

How to cite: Ospina, V., Buitrago-Sierra, R., & López, D. (2015). Hdo of guaiacol over NiMo catalyst supported on activated carbon derived from castor de-oiled dake. *Ingeniería e Investigación, 35(2)*, 49-55. DOI: http://dx.doi.org/10.15446/ing.investig.v35n2.49838

losic precursor during pyrolysis (Ioannidou & Zabaniotou, 2007), besides they serve as porogens. A number of studies have reported the production of activated carbons using the methods mentioned above and different sources of biomass such as olive stones (González *et al.*, 2009), palm shells (Adinata, Wan Daud, & Aroua, 2007), corn cob (Song et al., 2013), tea residues (Gurten, Ozmak, Yagmur, & Aktas, 2012) and others cellulosic based precursors.

During pyrolysis, char formation is not the only process that occur, liquid products which have potential application in the production of liquid fuels are also generated (Bykova *et al.*, 2012; Xiu & Shahbazi, 2012; Zhang, Zhang, *et al.*, 2013). However, some of their physicochemical characteristics demand additional upgrading processes that allow their use; one of these processes is hydrodeoxygenation (HDO). Bio-oils have a complex chemical composition. This is the reason why many authors have studied HDO reaction with model compounds including phenol (Zhang, Wang, Ma, Zhang, & Jiang, 2013), guaiacol (Ghampson *et al.*, 2012) among others instead of studying bio-oils directly, in order to understand the basic chemical behavior. In HDO, high temperatures, high pressures of H_2, and the use of hydrogenation and deoxygenation catalysts are applied in order to generate compounds similar to hydrocarbons. ACs from biomass can be used as catalyst support in HDO reactions (Sepúlveda *et al.*, 2011). Castor oil is widely used in industry. After its extraction, the disposal of the remaining solid management is challenging due to the presence of toxins such as ricin and ricinine (Barnes, Baldwin, & Braasch, 2009), therefore, it is significant to find a path to reutilize this waste, to generate add-on values. The aim of this work is to explore a one-pot synthesis solutions: by exploring both physical and chemical activation to convert castor de-oiled cake residue into useful ACs, which in-turn could be used as Ni-Mo catalyst supports for the HDO reaction.

Experimental

Materials: Castor seeds were donated by Colombian Biofuels SA (variety Nordestina BRS-149); after seeds are crushed, a by-product of castor oil, which is called de-oiled cake, is generated. The activating agents used were CO_2 (Linde, 99.8 %) and K_2CO_3 (Merck, > 99 %). The Ni and Mo precursors used in the synthesis of the catalysts were $Ni(NO_3)_2 \bullet 6H_2O$ (Panreac, 98 %) and $(NH_4)_6Mo_7O_{24} \bullet 4H_2O$ (Panreac, 99 %). For the hydrodeoxygenation reaction, hydrogen (Linde, 99.995 %), decalin (Merck, 99 %) as solvent, guaiacol (Sigma Aldrich. oxidation indicator) as model compound and commercial available sulfurizing agent SulfrZol® 54 (olefin sulfide, Lubrizol) were used. In order to establish some comparisons, reactions were performed with two commercial catalysts typically used in this kind of reactions, Haldor TopsØe TK-351 (Mo 15-24 wt %, Ni 2-5 wt %), named as HT-NiMo and KATALCO 61-T (Mo 7 wt %, Ni 2.8 wt %), named as KA-NiMo.

Supports and catalyst preparation: The activated carbon obtained by physical activation was made in two steps: biomass pyrolysis and char activation. The pyrolysis of the raw material was carried out in a horizontal furnace using a heating rate of 20 °C/min up to 800 °C for 1 h, the sample, after carbonization was cooled down and sieved to homogenize particle size between 75 µm and 180 µm, and then the char samples were brought back to the furnace for activation. As soon as the system had achieved 800 °C, nitrogen was replaced by the activating agent (steam saturated CO_2 at 80, 100 mL/min) and reaction was allowed for 2 hours. The AC was denominated P-AC (activated carbon by physical activation).

For chemical activation, the biomass was ground and sieved with 30 mesh (0.6 mm), and then impregnated with a solution of potassium carbonate under stirring considering a 1:1 weight ratio K_2CO_3: biomass during 24 hours at room temperature. Then the sample was dried in an oven at 110 °C. Finally, the sample was carbonized in N_2 using a heating rate of 20° C/min up to 800 °C for 1 h; after cooling down the sample was washed with distilled water to neutral pH. Prior to use the AC in the catalysts synthesis, it was crushed and sieved into the same particle size (75µm - 180 µm). The AC was denominated C-AC (activated carbon by chemical activation).

Catalysts were prepared by wet impregnation, using the right amount of each precursor ($Ni(NO_3)_2 \bullet 6H_2O$) and ($(NH_4)_6Mo_7O_{24} \bullet 4H_2O$), to obtain 2 wt% Ni and 10 wt% Mo of each metal in the catalyst. The AC supports were proportionally added to an aqueous solution of both salts, and kept for 14 h using a rotary evaporator at room temperature. After impregnation, the excess volume was removed by evaporation under vacuum for 3 h. The resultant sample was dried in air at 110 °C for 3 h and finally calcined in N2 with a heating rate of 10 °C/min up to 500 °C for 1 h (Campanati, Fornasari, & Vaccari, 2003). These catalysts were labeled as P-AC-NiMo and C-AC-NiMo, respectively.

Characterization: Proximate analysis was carried out in an automated thermogravimetric system using a TA Instruments Q500 TGA. Elemental analyses were performed using a TruSpec 630-200-200 CNHS-O Analyzer. The inorganic composition was determined in a Thermo Scientific ARL OPTIM'X WDXRF Analyzer. BET surface areas (S_{BET}), micropore ($V_{\mu p}$) and total (V_T) volumes**,** medium pore diameter (d_p) and pore size distributions of the ACs and catalysts were determined by nitrogen physisorption in a Micromeritics ASAP 2020. Infrared analysis was performed in a Shimadzu IR Affinity-1S FTIR spectrophotometer. Samples morphology and surface composition were characterized by SEM-EDS, using a JEOL JSM-6490LV Scanning Electron Microscope with EDX. TPR of hydrogen (H2-TPR) was performed in a 10 % H2 in Ar stream; the samples were heated up to a final temperature of 1000 °C at 10 °C/min and H_2 consumption was monitored by a thermal conductivity detector; the analyses were performed in a Micromeritics Autochem II 2920 equipment.

Guaiacol HDO reactions: HDO reactions were carried out at 350 °C, 5 MP_a and 100 rpm in a 25 mL stainless steel reactor (Ogawa 50), equipped with a magnetic stirrer and a furnace with electric temperature controller. The catalyst was sulfided in-situ, 0.1 g of catalyst with particle sizes ranging from

75 to 180 µm was introduced into the reactor followed by 0.08 g of sulfurizing agent addition, and finally about 0.57 g of GUA and 8.064 g of decalin ($C_{10}H_{18}$) were employed to set the reactant-solvent ratio close to 7 wt%. Afterwards, the reactor was sealed and purged two times to eliminate air, first argon was used then it was replaced by H_2. After that, the reactor was pressurized to the desired hydrogen pressure and heated to the desired temperature; by the time the system had reached the desired condition the reaction was left to run for 1h. Once the reaction was finished, the autoclave was cooled quickly to room temperature and brought to ambient pressure. The products were analyzed by gas chromatography coupled with mass spectrometry; products identification was achieved using a SHRXI-5MS (30 m x 0,25 mm x 0.25 µm) capillary column and a MS detector and quantification was made using a DB-5 (30 m × 0.32 mm × 0.5 m) capillary column and a FID detector. Tetradecane was used as internal standard, response factors were determined experimentally using pure compounds.The conversions of guaiacol and liquid products distribution were calculated based on the GC analysis. The conversion of guaiacol was calculated from the initial and final amounts of GUA, by the equation:

$$\%Conversion = \frac{nGUA_{in} - nGUA_{out}}{nGUA_{in}} * 100 \quad (1)$$

Where $nGUA_{in}$ is the initial amount of *GUA*, and $nGUA_{out}$ is the final amount of *GUA*.

Guaiacol HDO activity was calculated to compare the intrinsic activity of different catalysts, by the equation:

$$Activity = \frac{nGUA_{converted}}{n_{Ni+Mo} * h} \quad (2)$$

Where $nGUA_{converted}$ is the amount of *GUA* converted by each catalyst; n_{Ni+Mo} is the moles of both metals in the catalyst, and *h* is the time of the reaction.

Results and discussion

ACs characterization: the characteristics of biomass, char and ACs are shown in Table 1. A high oxygen content due polysaccharides such as cellulose and hemicellulose is observed (Huber, Iborra, & Corma, 2006). In addition, significant nitrogen content attributable to the presence of some proteins, particularly ricin, is also seen (Barnes *et al.*, 2009). There is a higher carbon content and a lower oxygen and hydrogen content in char than in biomass, this occurred because of heat treatment, when most of the oxygen in biomass becomes part of the pyrolysis liquid products. On the other hand, the char contains 12 wt. % oxygen, which remains in the char after the activation process. This leads to ACs having a variety of oxygen functional groups.

Table 1. Properties of biomass, bio-char and ACs

Property	Material			
	Biomass	Bio-char	P-ac	C-ac
Elemental (wt%)				
Carbon[a]	53.02	81.19	78.65	74.37
Nitrogen[a]	4.81	4.75	3.64	2.13
Oxygen*[a]	34.79	12.36	14.81	19.99
Hydrogen[a]	7. 28	1.38	2.80	3.43
Sulfur[a]	0.09	0.32	0.09	0.07
Proximate (wt%)				
Moisture[c]	3.6	5.4	1.7	32.9
Volatile matter[b]	89.9	7.8	3.1	15.8
Fixed carbon[b]	6.4	71.5	65.3	79.3
Ash[b]	2.9	20.2	31.4	5.1

[a] Dry-ash free basis. [b] Dry basis. [c] As received. * By difference.

Proximate analysis showed that biomass has a high percentage of volatile material, which is typical of this kind of materials (Ioannidou & Zabaniotou, 2007; Saldarriaga *et al.*, 2015), due to the breaking of the chemical bonds of cellulose, hemicellulose, lignin and fatty acids present in the biomass. CO, CO_2, CH_4 and a variety of volatile compounds such as alcohols, acids, phenols, among others are generated (Huber *et al.*, 2006; Singh & Shadangi, 2011).

The ash content, which can vary depending on the type of biomass and soil conditions where it is grown, is integral to the plants and involves a wide range of minerals such as calcium, potassium, silicon and magnesium, which are part of biomass structure (Singh & Shadangi, 2011). Fresh biomass, char, P-AC and C-AC were analyzed by X-ray fluorescence. The inorganic composition in biomass, char and P-AC consist of high phosphorus content, one of major nutrients in plants and metals such as Ca, K, Mg, etc. However, it is not the same for chemically activated carbon, which has shown a decrease in the percentage of the inorganic component (Table 1); the removal of mineral material occurs during washing after pyrolysis; in these sense the treatment with K_2CO_3, a basic substance, may favor demineralization.

IR spectra for the two ACs are shown in Figure 1. IR spectra of ACs give some information about the characteristics related to the chemical composition of the carbonaceous materials. In P-AC the most noticeable bands at 560–640 cm^{-1}, 870 cm^{-1} and 1050 cm^{-1} to 1100 cm^{-1}, could be associated to phosphate group ($PO4^{3-}$) (Rivera-muñoz, 2000), a typical inorganic constituent of biomass due to the presence of any Calcium phosphate . The presence in both ACs of functional groups related with the decomposition of cellulose, hemicellulose and lignin was confirmed. In both samples, wide and weak O-H stretching and C-OH stretching bands are shown around 3430 cm^{-1}, C-AC also exhibit signals around 1050 cm^{-1} and 1100 cm^{-1} which are attributed to the presence of alcohols or phenols, but in P-AC this signals are probably overlapped by the phosphate signal which is stronger. The absorption band around 3400 cm^{-1} corresponds to the stretching vibrations of OH and N-H groups; some authors have reported that as the pyrolysis temperature increases the band at 3400 cm^{-1} tends to disappear (Apaydın-Varol & Pütün, 2012).

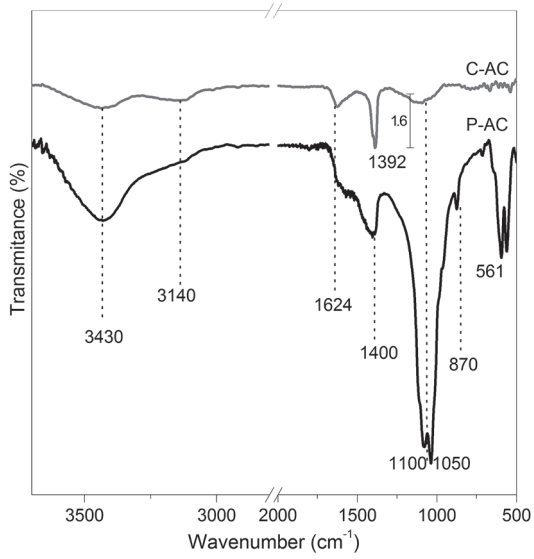

Figure 1. IR spectra for physically activated carbon (P-AC) and chemically activated carbon (C-AC)

Some bands observed that near 3140 cm^{-1} are typical of aliphatic, olefins. Further in C-AC the band in 1624 cm^{-1} can be attributed to olefinic structures while in P-AC the weak bands between 1600 cm^{-1} and 1500 cm^{-1} can be related to aromatic structures (Hernández & Bonilla, 2012). Both carbons show bands near to 1400 cm^{-1} that demonstrate the presence of aliphatic and terminal carbon bonds. It is possible that this sample has other chemical functionalities related to ether or carbonyl groups like ketones, aldehydes or esters; however, it is difficult to appreciate the characteristic bands due to the limitations of the samples.

To study the specific surface and the porosity of the samples, the standard N_2 adsorption method was carried out. The N_2 adsorption-desorption isotherm of the ACs are shown in Figure 2 (left). Both are typical type I isotherms according to IUPAC classification, C-AC isotherm presents a high adsorption at low relative pressure and exhibits a broad knee attribute to the co-existence of both micropores and mesopores in large numbers. However, it did not show a hysteresis loop indicating that C-AC is essentially a microporous material, while the isotherm for the activated carbon P-AC showed a hysteresis loop that evidences the presence of mesopores. Figure 2 (right) shows the pore size distribution of both ACs. It can be observed that the pore structure in these materials mainly consists of micropores.

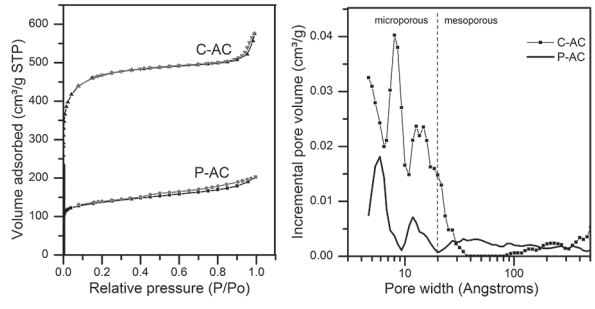

Figure 2. Adsorption/desorption isotherms of the activated carbons P-AC y C-AC (left) with DFT pore size distribution for P-AC y C-AC (right).

Table 2 summarizes the textural data of the samples where the characteristics observed in Figure 2 are quantified. BET surface areas of the activated carbons prepared by physical and chemical method, P-AC y C-AC, were 566 $m^2\ g^{-1}$ and 1510 $m^2\ g^{-1}$, respectively. For the activated carbon, C-AC the area obtained clearly reflects important effects of the microporosity on the total surface area. The sample P-AC exhibited the major medium pore diameter, but the minor microporous volume, therefore, the minor specific surface area.

Table 2. Textural data obtained by nitrogen isotherms, using BET and DFT methods

Samples	SBET ($m^2\ g^{-1}$)	Vμp (cc g^{-1})	VT (cc g^{-1})	dp (Å)
P-AC	566	0.1529	0.2590	27
C-AC	1510	0.5837	0.7942	23

SEM images of both ACs are shown in Figure 3. As can be seen from the micrographs, the AC obtained by physical activation (Figure 3, a and b) is a homogeneous material with particles exhibiting flat faces, wherein the porosity is not easily detectable. Furthermore, the material obtained by chemical activation (Figure 3, c and d) has a heterogeneous structure, showing apparent porosity because of the irregularity of the particles; a porous sponge-like structure can be clearly seen.

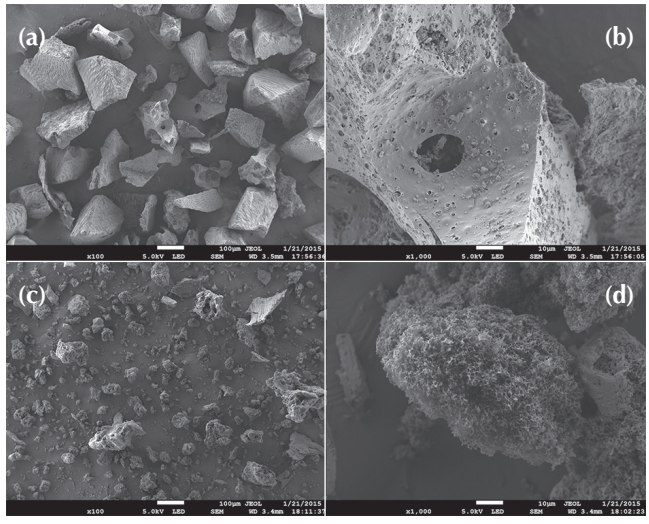

Figure 3. SEM micrographs for P-AC (a,b) and C-AC (c,d).

Catalyst characterization

As previously mentioned, one of the possible applications of these materials is their use as catalyst supports; (Chen *et al.*, 2014; Serp & Figueredo, 2009) considering catalysts design, a good dispersion of the inorganic phases over supports is required. In this sense the dispersion of Ni and Mo salts (Calafat & Laine, 1996; Ruiz *et al.*, 2012) on the ACs was evaluated. After impregnation and decomposition of the precursor, samples were analyzed by XRF in order to determine the Ni and Mo loads; values are given in Table 3. According to the theoretical load of Ni and Mo, it was possible to observe that Ni was deposited more

efficiently on the carbonaceous material, as the loading percentage of Ni in both synthesized catalysts was similar to the nominal. On the other hand, the load of Mo was lower for both catalysts in contrast to the nominal value. In spite of this, the catalyst prepared with C-AC showed a higher content of Mo, which can be attributed to a higher adsorption probably related to its high surface area.

In Table 3 the catalysts surface areas after metal impregnation are also shown. Typical decrease of the surface area attributed to the clogging of some pores after agglomerate formation on the supported phase was found.

Table 3. XRF and surface area analyses for the synthesized catalysts.

Metal loading	Ni (wt %)	Mo (wt %)	SBET (m^2 g^{-1})
Theoretical	2	10	---
P-AC-NiMo	2.4	5.0	410
C-AC-NiMo	2.1	7.3	1031
HT-NiMo	7.0	22.1	240
KA-NiMo	3.3	7.3	265

In order to explore the chemical composition on the ACs surface, both samples were subjected to a study by SEM-EDS (not show, see (Ospina-guarín, Buitrago-sierra, & López-lópez, 2014)). The presence of K, Ca, Mg, P and typical inorganic components in biomass was determined by EDS; the loaded metals were found 2.74 % Ni and 8.77 % Mo for P-AC-NiMo and 1.75 % Ni and 8.24 % Mo for C-AC-NiMo, values that agree with theoretical ones proposed in the carbonaceous support material and XRF results. Ni and Mo species were homogeneously distributed on the ACs surface and no aggregates could be observed as can be concluded from SEM-EDX images.

Reducibility is a characteristic related to the ability of the catalyst to form an active phase in a reductive atmosphere. In Figure 4 the TPR curves for the supports and catalysts are shown. Activated carbon P-AC show two reduction events at 632 °C and 796 °C that are attributed to the oxygen species in the carbonaceous material which leads the CO_2 or CO formation from O-containing functional groups on the surface of AC supports (Jin *et al.*, 2014), they are also related to carbon methanation. If this idea is contrasted with the IR spectrum, a match of the oxygen groups present in the material can be suggested. The first reduction peak should correspond to the easy reduction of carbonyl groups while the second peak should correspond to the hydroxyl groups. If the same analysis is made for C-AC-NiMo, which shows a single reduction event at 605 °C, the symmetry of the curve may suggest that multiple reduction events overlap. Nevertheless, it is inferred that this activated carbon is less oxidized, this is why is reduced at lower temperatures. It is important to note that if the percentage of H_2 consumption by the support in the catalyst reduction is considered, then it can be determined that the support is responsible for 53 % H_2 consumption in P-AC-NiMo and 41 % H_2 consumption in C-AC-NiMo.

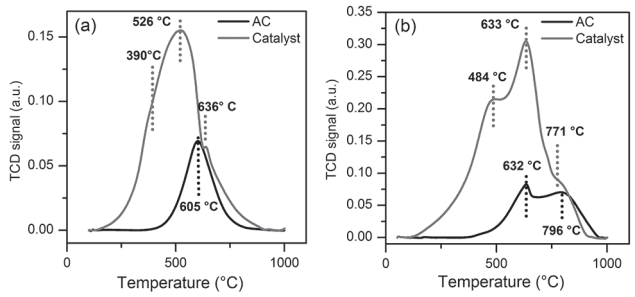

Figure 4. TPR curves for the synthetized catalysts C-AC-NiMo (a) and P-AC-NiMo (b) and their respective carbonaceous supports.

On the other hand, the P-AC-NiMo TPR profile shows the presence of several reducible species. In the figure, the peak at 484 °C could be related with the reduction of Ni and Mo species, additionally, the oxidized species cannot be clearly explained. It has been reported that Ni species are reduced at about 450 °C, furthermore, signals at low temperature are usually related to the reduction of NiO clusters weakly interacting with the support, while higher temperatures are for highly dispersed NiO with stronger interactions (Jin *et al.*, 2014) and Mo species at about 500 °C (Calafat & Laine, 1996). There are some studies in which the reduction of both species supported on mesoporous carbon occur at lower temperatures (Prabhu, Dalai, & Adjaye, 2011). In the case of the catalyst prepared with C-AC it is seen that reducible inorganic species are present with maximum H_2 consumption at 524 °C.

Hydrodeoxygenation Reaction of Guaiacol

GUA conversion results are presented in Figure 5a, in this, a thermal conversion of 10 % is seen, it can also be concluded that the ACs have minimum impact on the reaction, since the conversion was similar to the one observed by thermal conversion. Commercial catalysts have a higher metal load content, and thus show the highest conversion rates; nevertheless, the synthesized catalysts are also active in the HDO reaction. However, when the intrinsic catalytic activity of the commercial and synthesized catalysts is compared, it is observed that C-AC-NiMo exhibits better activity compared to commercial catalysts, and P-AC-NiMo has activity comparable to the commercial catalyst, even higher than H. Topsoe. The routes for guaiacol HDO are primarily determined by the methoxy group, the hydroxyl group and the aromatic ring (He & Wang, 2012). Demethylation (breaking of the O-methyl bond) to give catechol and subsequent deoxygenation leads to phenol formation, followed by CO hydrogenolysis and aromatic ring hydrogenation to give cyclohexene and cyclohexane. In our reactions the major products were phenol, catechol, cyclohexanone, cyclohexane, cyclohexene, which agrees with some studies reported in specialized literature (Ghampson *et al.*, 2012).

In Figure 5b. product distribution is also shown. In reactions without catalyst and ACs, catechol was the main product, indicating that the thermal degradation of the com-

pound leads to guaiacol demethylation. In reactions with both commercial and synthesized catalysts, phenol was the major product, nevertheless in reactions with P-AC-NiMo and C-AC-NiMo, the product distribution showed increased formation of cyclohexane and cyclohexene, indicating that these catalysts favor formation of non-oxygenated and saturated compounds, one of the main objectives in this kind of process. There may be several reasons to explain this behavior, and some of them may be associated with the catalyst support.

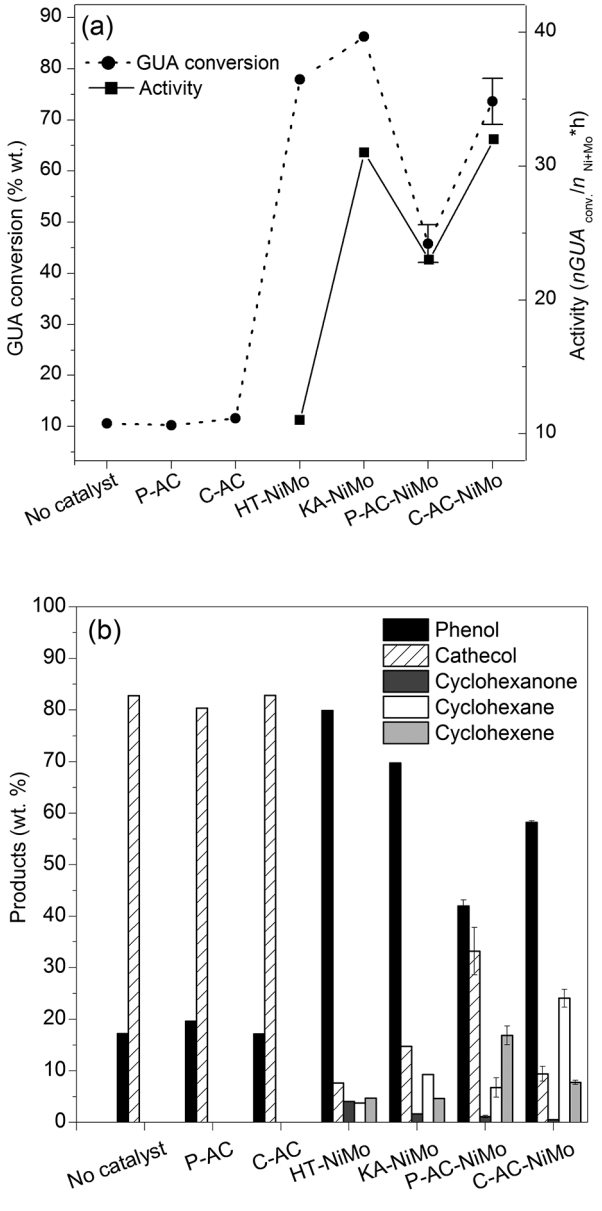

Figure 5. Guaiacol conversion and catalyst activity (a). Liquid products distribution of guaiacol HDO (b).

The commercial catalysts used for comparison were NiMo supported on alumina, and considering that alumina by itself can convert guaiacol phenol and catechol by its acidic nature (8-10 times less active sulfides) (Bui, Laurenti, Delichère, & Geantet, 2011). Part of the conversion can be associated to the support activity. On AC supported catalyst, no catalytic activity was experimentally observed, which accounts for its inert character. Furthermore the interaction between the active phase and the support, in the case of alumina is higher than the interaction with AC (Serp & Figueredo, 2009), which can facilitate reducing the active phase and the interaction of the reactants with the active phase. However, the most important feature of the support is the AC high surface area compared with alumina, which also increases the interaction between the active phase and the reagents.

Conclusions

De-oiled castor cake is a suitable material for the production of value-added activated carbon from biomass. ACs produced by physical and chemical activation showed differences in morphology that was reflected in surface areas. C-AC exhibited better performance with a larger surface area. It was also found that the methodology of preparation for C-AC promotes a reduction in ash content. Potential use of ACs as catalyst support was confirmed by observing the high dispersion of the inorganic phase in the ACs and their efficiency in removing oxygen and saturated compounds formation. Commercial catalysts tested showed greater Guaiacol conversion; however, the synthesized catalysts showed higher activity towards the formation of products such as cyclohexane and cyclohexene, meaning that they favor the hydrogenation and deoxygenation.

Acknowledgments

The authors acknowledge to the University of Antioquia for the financial support through Programa Sostenibilidad 2014-2015, and CODI for financing the project No. 01540.

References

Abdullah, N., Sulaiman, F., & Gerhauser, H. (2011). Characterisation of Oil Palm Empty Fruit Bunches for Fuel Application. *Journal of Physical Science, 22(1)*, 1–24.

Adinata, D., Wan Daud, W.M.A., & Aroua, M.K. (2007). Preparation and characterization of activated carbon from palm shell by chemical activation with K_2CO_3. *Bioresource Technology, 98(1)*, 145–9. DOI:10.1016/j.biortech.2005.11.006

Apaydın-Varol, E., & Pütün, A.E. (2012). Preparation and characterization of pyrolytic chars from different biomass samples. *Journal of Analytical and Applied Pyrolysis, 98*, 29–36. DOI:10.1016/j.jaap.2012.07.001

Auer, E., Freund, A., Pietsch, J., & Tacke, T. (1998). Carbons as supports for industrial precious metal catalysts. *Applied Catalysis A: General, 173(2)*, 259–271. DOI:10.1016/S0926-860X(98)00184-7

Barnes, D.J., Baldwin, B.S., & Braasch, D.A. (2009). Ricin accumulation and degradation during castor seed development and late germination. *Industrial Crops and Products, 30(2)*, 254–258. DOI:10.1016/j.indcrop.2009.04.003

Bridgwater, A.V. (2011). Review of fast pyrolysis of biomass and product upgrading. *Biomass and Bioenergy*, 38, 68–94 DOI:10.1016/j.biombioe.2011.01.048

Bui, V.N., Laurenti, D., Delichère, P., & Geantet, C. (2011). Hydrodeoxygenation of guaiacol. *Applied Catalysis B: Environmental, 101(3-4)*, 246–255. DOI:10.1016/j.apcatb.2010.10.031

Bykova, M.V., Ermakov, D.Y., Kaichev, V.V., Bulavchenko, O.A., Saraev, A.A., Lebedev, M.Y., & Yakovlev, V.A. (2012). Ni-based sol–gel catalysts as promising systems for crude bio-oil upgrading: Guaiacol hydrodeoxygenation study. *Applied Catalysis B: Environmental, 113-114*, 296–307 DOI:10.1016/j.apcatb.2011.11.051

Calafat, A., & Laine, J. (1996). Effect of Surface Oxidation of the Support on the Thiophene Hydrodesulfurization Activity of Mo , Ni , and NiMo Catalysts Supported on Activated Carbon. *Journal of Catalysis, 162*, 20–30.

Campanati, M., Fornasari, G., & Vaccari, A. (2003). Fundamentals in the preparation of heterogeneous catalysts. *Catalysis Today, 77(4)*, 299–314. DOI:10.1016/S0920-5861(02)00375-9

Chen, W., Luo, Z., Yu, C., Yang, Y., Li, G., & Zhang, J. (2014). Catalytic conversion of guaiacol in ethanol for bio-oil upgrading to stable oxygenated organics. *Fuel Processing Technology, 126*, 420–428. DOI:10.1016/j.fuproc.2014.05.022

Ghampson, I.T., Sepúlveda, C., Garcia, R., Radovic, L.R., Fierro, J.L.G., DeSisto, W.J., & Escalona, N. (2012). Hydrodeoxygenation of guaiacol over carbon-supported molybdenum nitride catalysts: Effects of nitriding methods and support properties. *Applied Catalysis A: General, 439-440*, 111–124. DOI:10.1016/j.apcata.2012.06.047

González, J.F., Román, S., Encinar, J.M., & Martínez, G. (2009). Pyrolysis of various biomass residues and char utilization for the production of activated carbons. *Journal of Analytical and Applied Pyrolysis, 85(1-2)*, 134–141. DOI:10.1016/j.jaap.2008.11.035

Gurten, I.I., Ozmak, M., Yagmur, E., & Aktas, Z. (2012). Preparation and characterisation of activated carbon from waste tea using K_2CO_3. *Biomass and Bioenergy, 37*, 73–81. DOI:10.1016/j.biombioe.2011.12.030

He, Z., & Wang, X. (2012). Hydrodeoxygenation of model compounds and catalytic systems for pyrolysis bio-oils upgrading. *Catalysis for Sustainable Energy, 1*, 28–52. DOI:10.2478/cse-2012-0004

Hernández, V., & Bonilla, A. (2012). *Lignocellulosic Precursors used in the Synthesis of Activated Carbon - Characterization Techniques and Applications in the Wastewater Treatment*. Croatia: InTech.

Huber, G.W., Iborra, S., & Corma, A. (2006). University of Massachusetts - Amherst Synthesis of Transportation Fuels from Biomass: Chemistry, Catalysts, and Engineering. *Chemical Reviews, 106(9)*, 4044–4098.

Ioannidou, O., & Zabaniotou, A. (2007). Agricultural residues as precursors for activated carbon production—A review. *Renewable and Sustainable Energy Reviews, 11(9)*, 1966–2005. DOI:10.1016/j.rser.2006.03.013

Jin, S., Xiao, Z., Li, C., Chen, X., Wang, L., Xing, J., … Liang, C. (2014). Catalytic hydrodeoxygenation of anisole as lignin model compound over supported nickel catalysts. *Catalysis Today, 234*, 125–132. DOI:10.1016/j.cattod.2014.02.014

Kazehaya, A., Muroyama, K., & Watkinson, A.P. (2000). Preparation of activated carbon from lignin by chemical activation. *Carbon, 38*, 1873–1878.

Marsh, H., & Rodriguez-reinoso, F. (2006). *Activated Carbon*. Elsevier Science & Technology Books.

Ospina-guarín, V. M., Buitrago-sierra, R., & López-lópez, D. P. (2014). Preparation and characterization of activated carbon from castor de-oiled cake. *Tecno Lógicas*, *17(32)*, 75–84.

Prabhu, N., Dalai, A. K., & Adjaye, J. (2011). Hydrodesulphurization and hydrodenitrogenation of light gas oil using NiMo catalyst supported on functionalized mesoporous carbon. *Applied Catalysis A: General, 401(1-2)*, 1–11. DOI:10.1016/j.apcata.2011.04.019

Rivera-muñoz, E. M. (2000). Hydroxyapatite-Based Materials : Synthesis and Characterization. *Biomedical Engineering - Frontiers and Challenges*, 1–25. DOI:10.5772/19123

Ruiz, P. E., Frederick, B. G., De Sisto, W. J., Austin, R. N., Radovic, L. R., Leiva, K., … Wheeler, M. C. (2012). Guaiacol hydrodeoxygenation on MoS_2 catalysts Influence of activated carbon supports. *Catalysis Communications, 27*, 44–48.

Saldarriaga, J. F., Aguado, R., Pablos, A., Amutio, M., Olazar, M., & Bilbao, J. (2015). Fast characterization of biomass fuels by thermogravimetric analysis (TGA). *Fuel, 140*, 744–751. DOI:10.1016/j.fuel.2014.10.024

Sepúlveda, C., Leiva, K., García, R., Radovic, L. R., Ghampson, I. T., DeSisto, W. J., … Escalona, N. (2011). Hydrodeoxygenation of 2-methoxyphenol over Mo2N catalysts supported on activated carbons. *Catalysis Today*, *172(1)*, 232–239. DOI:10.1016/j.cattod.2011.02.061

Serp, P., & Figueredo, J. L. (2009). *Carbon Materials for catalysis*. John Wiley & Sons, Inc.

Singh, R. K., & Shadangi, K. P. (2011). Liquid fuel from castor seeds by pyrolysis. *Fuel, 90(7)*, 2538–2544. DOI:10.1016/j.fuel.2011.03.015

Song, M., Jin, B., Xiao, R., Yang, L., Wu, Y., Zhong, Z., & Huang, Y. (2013). The comparison of two activation techniques to prepare activated carbon from corn cob. *Biomass and Bioenergy*, 48(800e1000 C), 250–256. DOI:10.1016/j.biombioe.2012.11.007

Xiu, S., & Shahbazi, A. (2012). Bio-oil production and upgrading research: A review. R*enewable and Sustainable Energy Reviews, 16(7)*, 4406–4414. DOI:10.1016/j.rser.2012.04.028

Zhang, X., Wang, T., Ma, L., Zhang, Q., & Jiang, T. (2013). Hydrotreatment of bio-oil over Ni-based catalyst. *Bioresource Technology, 127*, 306–311. DOI:10.1016/j.biortech.2012.07.119

Zhang, X., Zhang, Q., Wang, T., Ma, L., Yu, Y., & Chen, L. (2013). Hydrodeoxygenation of lignin-derived phenolic compounds to hydrocarbons over Ni/SiO_2-ZrO_2 catalysts. *Bioresource Technology, 134*, 73–80. DOI:10.1016/j.biortech.2013.02.039